



CARMA Memorandum Series #52

Aperture Efficiency, Pointing and Primary Beam Calibration.

Melvyn Wright¹, David MacMahon¹, Stuartt Corder² & Göran Sandell³

*Radio Astronomy Laboratory, U.C. Berkeley¹; ALMA²;
Universities Space Research Association³.*

June 29, 2009

ABSTRACT

In this memo we present an analysis of observations of compact sources in an interferometer mosaic pattern to determine the aperture efficiency, pointing, and primary beam width for the CARMA antennas. The data are self-calibrated to determine the antenna voltage gains. Gaussian fits to the antenna voltage patterns are used to analyze the CARMA beam patterns at 100 & 230 GHz. For multichannel observations the antenna bandpass solutions are also obtained.

Using a hexagonal 7-pointing mosaic pattern works very well at 100 GHz. At 230 GHz good atmospheric phase stability is required to obtain reliable results. We measure antenna gains close to 65 and 145 Jy/K corresponding to aperture efficiencies 50% and 65% respectively for 10 and 6m antennas. At 100 GHz the data are consistent with a common FWHM for azimuth and elevation axes. The average FWHM for 10m antennas is 1.20 ± 0.02 arcmin. The average for 6m antennas is 1.98 ± 0.03 arcmin. These values are significantly larger than the the current Gaussian primary beam model FWHM; 1.07 and 1.92 arcmin for 10m and 6m antennas respectively. At 230 GHz the FWHM on the elevation axis appears to be smaller than on the azimuth for several of the antennas. This is possibly caused by gravitational deformation in both 6m and 10m antennas. The mean values are, azimuth: 0.55 ± 0.02 , elevation: 0.50 ± 0.02 for 10m antennas, and azimuth: 0.86 ± 0.02 , elevation: 0.83 ± 0.03 for 6m antennas.

In principle, we obtain an absolute gain calibration using planet observations with a planet model. However, if the planet is resolved then the derived gains depend on the detailed surface brightness distribution in the planet model, and may not produce reliable fits for the aperture efficiency or primary beamwidth. For use as an absolute flux density calibration, correction must be made for absorption lines in planetary atmospheres.

Change Record

Revision	Date	Author	Sections/Pages Affected
			Remarks
1.1	2009-June-01	MCHW	1-14
			Draft memo
1.2	2009-June-15	MCHW	1-19
			Draft memo
1.3	2009-June-17	MCHW	1-23
			added observing log
1.4	2009-June-17	MCHW	1-23
			mean and rms using smongo
1.5	2009-June-18	MCHW	1-23
			add to abstract and conclusion
1.5	2009-June-25	MCHW	24-25
			added 09JUN24 carma/ct007.1E_1003C273.1 data
1.5	2009-June-29	MCHW	24-25
			minor edits.

1. INTRODUCTION

Measurements of the aperture efficiency, antenna pointing and primary beamwidth are essential for quantitative calibration of astronomical images. An aperture synthesis array samples the cross correlation of the signals from an array of antennas, (or phased array stations in the case of the SKA). The signal from each antenna station measures the sky brightness distribution weighted by the antenna voltage pattern.

For a point source at the pointing center, e.g. a quasar calibration observation, the array response is well described by the forward gain and aperture efficiency. Accurate measurements of the forward gain require good pointing calibration. For an extended source distribution, the array response also depends on the primary beam illumination of the sky for each station pair.

The CARMA telescope is a heterogeneous array, with six 10.4 m, and nine 6.1 m antennas. The different antenna diameters and primary beam sizes allow regions up to $\sim 32''$ diameter to be observed with a single pointing center at 230 GHz. Regions up to $\sim 64''$ diameter can be observed with a 7-pointing hexagonal mosaic. Because of the different primary beam patterns, imaging with a heterogeneous array must be treated as a mosaic observation even when only a single pointing center is used for all antennas.

Images of the sky brightness are formed by combining the measured cross correlations between the antennas. The usual assumption for aperture synthesis imaging is that the illumination of the sky by the primary beam pattern is invariant, and the same for all antennas, then an image of the primary beam weighted sky brightness can be formed from a Fourier transform of the measured cross correlations.

The effects of amplitude and phase errors in the calibration of the measured cross correlations are well known. Less well appreciated are the effects of using the wrong primary beam illumination for an extended source distribution. The case for a homogeneous array of antennas has been well studied. The image fidelity for mosaic observations is limited by pointing and primary beam errors (Cornwell, Holdaway & Uson, 1993; Holdaway, 1998). For a heterogeneous array, it is necessary to determine the primary beam pattern for each antenna, in order to obtain accurate images.

In this memo we present observations using a 7-pointing hexagonal mosaic to determine the aperture efficiency, pointing, and primary beam width of the CARMA antennas. The integrated observing sequence provides antenna gains, and primary beamwidth corrected for pointing.

2. OBSERVATIONS AND DATA REDUCTION

Mosaic observations were obtained using a standard hexagonal 7-pointing mosaic of a strong compact source at the nominal pointing center and half power points for the 10m antennas. The data are self-calibrated to determine the antenna voltage gains. For quasars we used the MIRIAD task **mfc**al to determine the antenna-based gains versus time and bandpass. The voltage gains are determined for each pointing separately with respect to the flux density of the quasar. The ruby script **gpfit.rb** was used to make Gaussian fits to the voltage gains to determine the pointing and primary beam width of each of the the CARMA antennas.

For strong sources, **mfc**al also determines the bandpass from the channel data. For weaker sources, e.g. at 230 GHz on a 4 Jy source, we can use `line=wide`, which is currently 6 x 500 MHz channels to beat down the noise in the gains.

The ruby script **gpfit.rb** makes tables of the peak value, pointing offset and voltage primary beamwidth from the Gaussian fits to the antenna gains for each antenna and solution interval. Tables and plots at 100 GHz and 230 GHz are shown below.

Observation Log:

1) 06DEC20:07:29:12.0 File: ct006.3c111.2006dec20.1.miriad

13-pointing mosaic on 3c111 at 93/97 GHz. 500 MHz bandwidth. Total observing time 2.56 hours. Early attempt to measure the effect of mapping out to the 5% point in the primary beam by observing a strong compact source (the 3C111 nucleus), in an extended mosaic pattern. The image fidelity at the 5% points was severely degraded by primary beam errors, and good Gaussian fits to the primary beamwidth were not obtained.

(`gpfit.rb vis='*.*.uv' options=verbose,radecgpfit.rb vis='*.*.uv' options=verbose,azel`)
See Figure 1.

The panels on several of the antennas were later adjusted.

Reasonable fits were obtained for some antennas using only the 9 innermost pointings:

(`gpfit.rb vis='--0.0.uv,-14.09.-24.41.uv,14.09.24.41.uv,-14.09.24.41.uv,14.09.-24.41.uv,-28.19.0.uv,28.19.0.uv,-60.0.uv,60.0.uv' options=verbose > hex9.azel.fit`)

See Figure 2.

For several of the 6m antennas the fitted FWHM are not good.

2) 09MAR01:21:27:25.0 File: 0237+288

An "accidental" 19-pointing mosaic on the phase calibrator 0237+288 (thanks to Tony Wong for providing this data!).

Total observing time is 1.56 hours.

These observations, spanning 3 hours at 62 MHz bandwidth at

109/114 GHz on 0237+288, don't have enough SNR to do a Gaussian fit in a time

short compared with the phase variations with time. Although reasonable images of the calibrator could be made at each pointing, the Gaussian fits to determine the primary beamwidth were not reliable.

3) 09MAR31:13:29:45.5 File: ct007.1D_2303C454.1.miriad

7-pointing mosaic on 3C454.3 at 223/229 GHz with 500 MHz bandwidth.

Unfortunately using Nyquist sample interval for 100 GHz observations !

Good fits were not obtained with sample points at the 5% points in the primary beam pattern.

Total observing time 2.43 hours. 3 x 50 min intervals are shown.

See Figure 3.

4) 09APR17:04:06:49.0 File: ct007.1C_1003C273.1.miriad

7-pointing mosaic at 95/100 GHz with 500 MHz BW. Total observing time 0.73 hours

See Table 1 and Figure 4.

5) 09APR18:03:23:44.0 File: ct007.1C_1003C273.2.miriad

7-pointing mosaic at 95/100 GHz with 500 MHz BW. Total observing time 0.89 hours

See Table 2 and Figure 5.

6) 09APR26:07:00:41.5 File: ct007.1C_2303C273.1.miriad

7-pointing mosaic at 230 GHz with 500 MHz BW. Total observing time 0.83 hours

See Table 3 and Figure 6.

7) 09APR29:06:15:14.0 File: ct007.1C_2303C273.2.miriad

7-pointing mosaic at 223/229 GHz with 500 MHz BW. Total observing time 0.80 hours

See Table 4 and Figure 7.

8) 09MAY28:11:06:45.0 File: ct001.1C_230Neptune.2.miriad

7-pointing mosaic at 223/229 GHz with 500 MHz BW. Total observing time 1.23 hours

See Table 5.

9) 09JUN24:23:22:35.5 File: ct007.1E_1003C273.1.mir

7-pointing mosaic at 95/100 GHz with 500 MHz BW. Total observing time 0.70 hours

See Table 6.

Example of data reduction for a 7-pointing mosaic on a 3.9 Jy source.

```
#!/bin/csh -vf

# 230 GHz hexagonal mosaic on 4 Jy source.

# Use line=wide
    i.e. 6 x 500 MHz channels to beat down the noise in the gains.

# The integration times in mfc1 must chosen to give the same number of
solution intervals for each pointing.

echo "integration times chosen to give Number of solution intervals: 3,2,1"
foreach INT ( 50 100 10000)
    echo "integration time = $INT"
    foreach FILE ( --0.0 30.0 -30.0 15.26 -15.26 15.-26 -15.-26 )
        mfc1 vis=$FILE.uv flux=3.9 interval=$INT,$INT line=wide
    end
    gpfit.rb vis='*.*.uv' options=verbose > gpfit.$INT
    plotpbfits.rb -r 0.6 -n 4,4 -d /xs gpfit.$INT
    plotpbfits.rb -r 0.6 -n 4,4 -d gpfit.$INT.ps/ps gpfit.$INT
end
```

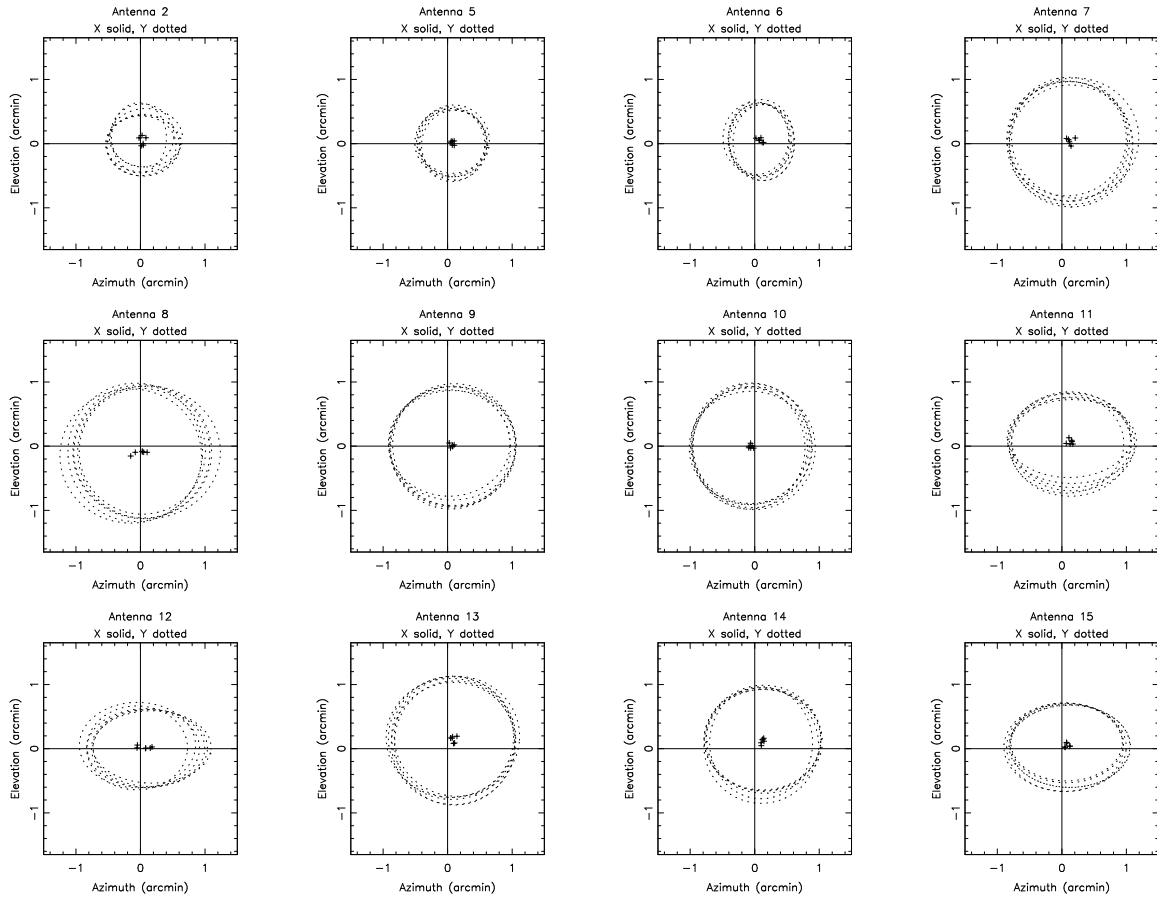


Fig. 1.— Pointing and Primary Beam FWHM at 93/97 GHz. 06DEC20. 13-pointing mosaic on 3c111. Figure shows the measured pointing (+), and Gaussian FWHM fits for 6 solution intervals over the 3 hour observation. Using longer solution intervals, the averaged voltage gains were spoiled by phase variations.

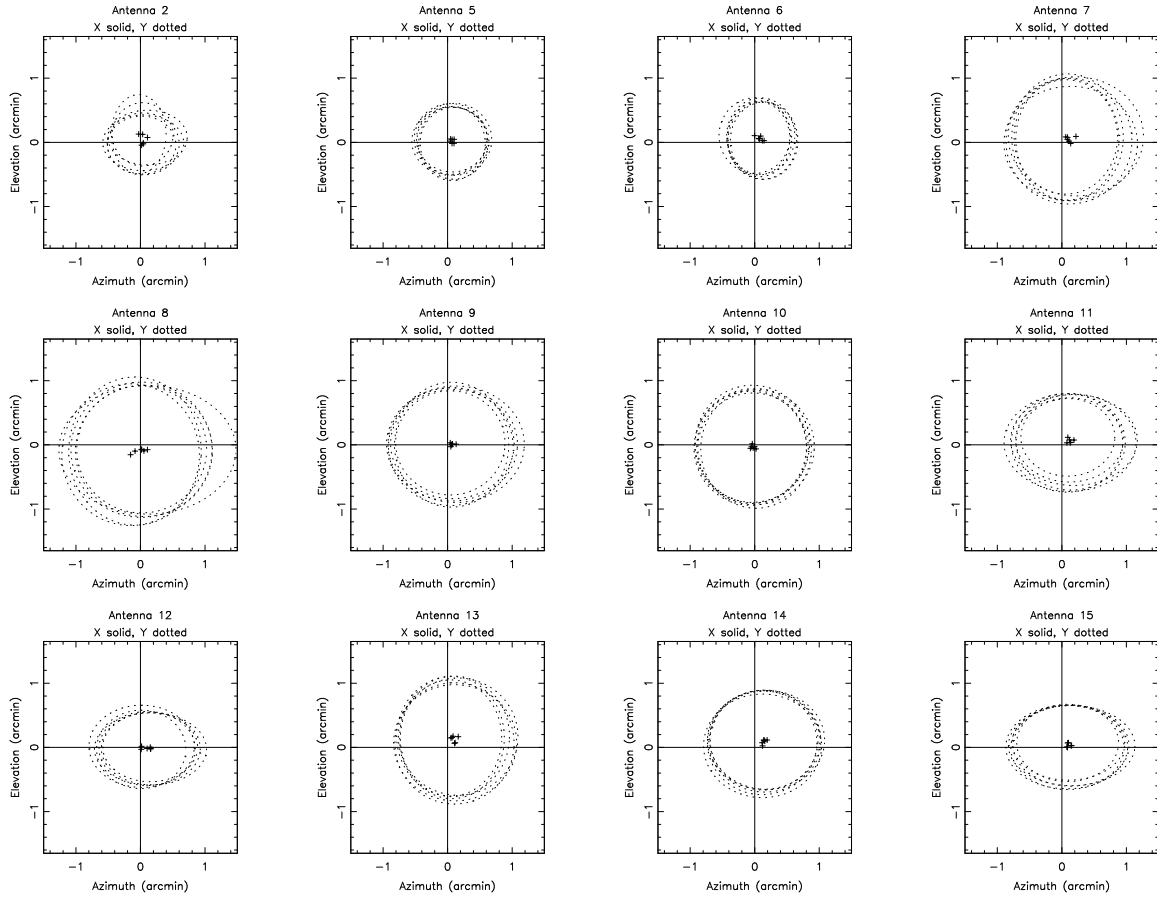


Fig. 2.— Pointing and Primary Beam FWHM at 93/97 GHz. 06DEC20. 9-pointing mosaic on 3c111 using the inner pointings.

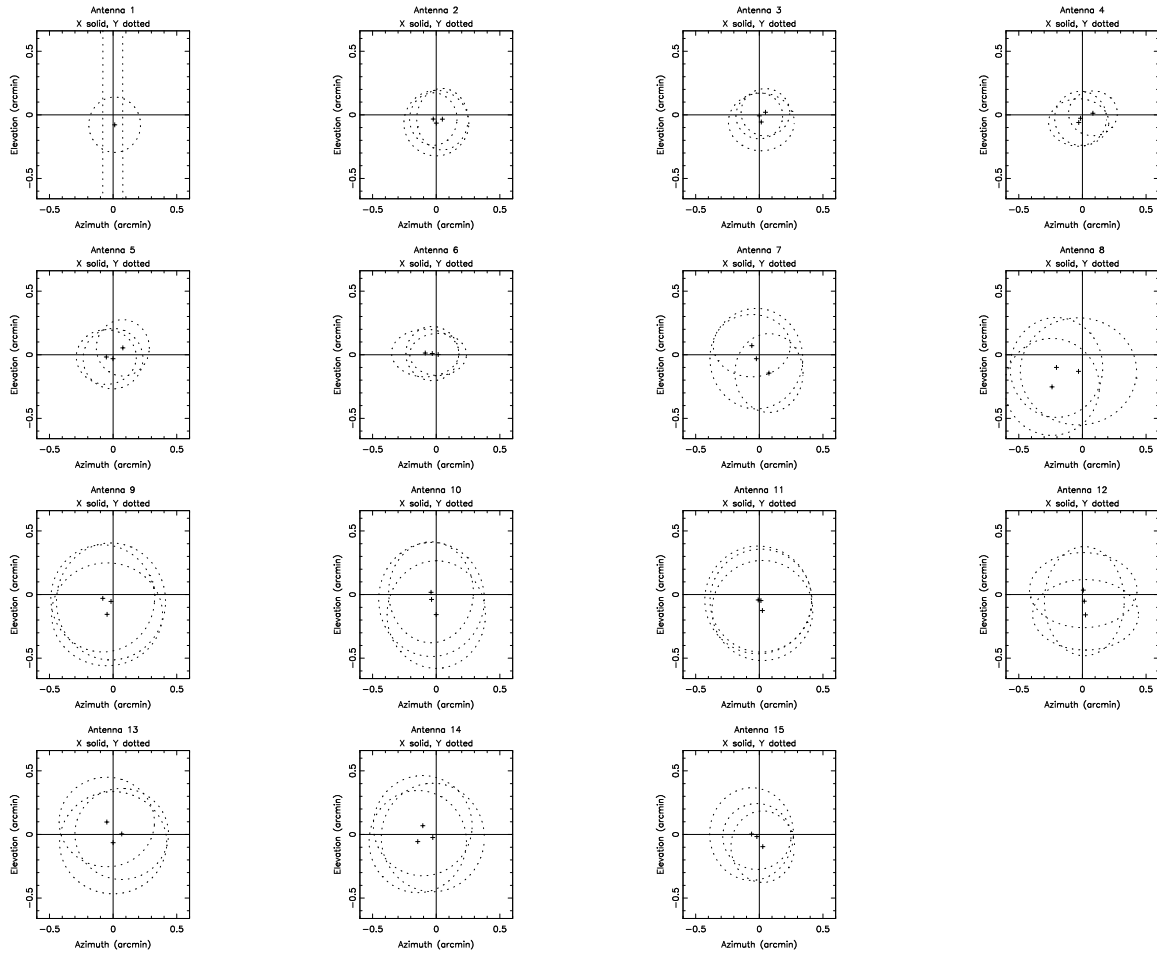


Fig. 3.— Pointing and Primary Beam FWHM using 3C454.3 at 230 GHz. 09MAR31. Total observing time 2.43 hours. Fits for 3 x 50 min intervals are shown. There are significant pointing variations between the 3 x 50 min intervals. Pointing variations within the 50 min measurement at each of the pointing positions degrade the Gaussian fits to the primary beamwidth.

3. ANALYSIS

3.1. CARMA antenna efficiencies

Tables 1 & 2 and Figures 4 & 5 show the results for 2 observations on 3C273 at 100 GHz. Tables 3 & 4 and Figures 6 & 7 show the results for 2 observations on 3C273 at 230 GHz.

The aperture efficiencies can be calculated from the peak values (*pkval*) fitted to the hex7 voltage patterns (and therefore corrected for pointing)

The peak values are w.r.t. the measured flux density for 3c273 and the nominal *jyperk* values in the data

The *jyperk* in the uv data are 65 and 145.337 for 10 and 6m antennas, corresponding to aperture efficiencies $32.5/65 = 50\%$ and $94.5/145.337 = 65\%$ respectively.

Using a flux for 3c273, 10 Jy at 230 GHz and 22 Jy at 100 GHz gives a peak value around 1, consistent with the nominal aperture efficiencies for 10 and 6m antennas. Lower peak values imply lower aperture efficiency. At 230 GHz, antennas 6, 10, and 15 have lower aperture efficiency.

gpfit.rb - Fit Gaussian primary beam to hex7 observational data.

aperture efficiency

$$10m(230GHz) = pkval^2 \times (10/Flux3c273) \times 50$$

$$10m(100GHz) = pkval^2 \times (22/Flux3c273) \times 50$$

$$6m(230GHz) = pkval^2 \times (10/Flux3c273) \times 65$$

$$6m(100GHz) = pkval^2 \times (22/Flux3c273) \times 65$$

3.2. CARMA primary beamwidths

The primary beamwidth is fitted in azimuth and elevation. Significant ellipticity is observed in some antennas. If we get consistent results we should change the nominal FWHM. Since these observations are similar to mosaic projects we should get better mosaic imaging performance using the measured primary beam FWHM. In Figure 8, we plot the fitted FWHM for all the measured antennas. At 100 GHz the data are consistent with a common FWHM for azimuth and elevation axes. The average FWHM for 10m antennas is 1.20 ± 0.02 arcmin. The average for 6m antennas is 1.98 ± 0.03 arcmin. These values are significantly larger than the the current Gaussian primary beam model FWHM 1.07 and 1.92 arcmin for 10m and 6m antennas respectively.

At 230 GHz the FWHM on the elevation axis appears to be smaller than on the azimuth for several of the antennas. This is possibly caused by gravitational deformation in both 6m and 10m antennas. More extensive observations at several telescope elevations are required to investigate this.

The mean values from the two 3C273 datasets (Tables 3 & 4) are: azimuth: 0.55 ± 0.02 arcmin, elevation: 0.50 ± 0.02 arcmin for 10m antennas, and azimuth: 0.86 ± 0.02 arcmin, elevation: 0.83 ± 0.03 arcmin for 6m antennas. The current Gaussian primary beam model has the same FWHM for both axes: FWHM 0.47 and 0.83 arcmin for 10m and 6m antennas respectively.

 Table 1. ct007.1C_1003C273.1.gpfit.0.2

#ant	pol	fit	iters	:	pkval	az_off	el_off	az_fwhm	el_fwhm	residual	
#####											
01	I	fit	1	iters	7	: 9.96e-01	-0.072	-0.034	1.162	1.224	X = 0.0151
02	I	fit	1	iters	7	: 1.00e+00	-0.016	0.020	1.198	1.167	X = 0.0198
03	I	fit	1	iters	7	: 1.04e+00	-0.041	-0.065	1.148	1.183	X = 0.0076
04	I	fit	1	iters	7	: 9.77e-01	-0.036	-0.030	1.227	1.221	X = 0.0128
05	I	fit	1	iters	7	: 9.63e-01	-0.051	-0.088	1.216	1.203	X = 0.0180
06	I	fit	1	iters	7	: 9.80e-01	-0.006	-0.007	1.216	1.195	X = 0.0203
07	I	fit	1	iters	8	: 9.75e-01	0.005	-0.034	2.044	1.948	X = 0.0032
08	I	fit	1	iters	9	: 9.61e-01	0.007	-0.075	2.055	2.160	X = 0.0083
09	I	fit	1	iters	9	: 9.48e-01	0.032	-0.007	1.841	1.950	X = 0.0142
10	I	fit	1	iters	8	: 9.55e-01	0.019	-0.142	1.920	1.991	X = 0.0036
11	I	fit	1	iters	8	: 9.98e-01	0.053	-0.030	1.944	1.989	X = 0.0087
12	I	fit	1	iters	8	: 9.51e-01	-0.026	-0.105	1.972	2.022	X = 0.0043
13	I	fit	1	iters	8	: 9.77e-01	0.043	-0.083	1.911	1.915	X = 0.0050
14	I	fit	1	iters	8	: 9.57e-01	-0.021	0.023	1.906	1.945	X = 0.0139
15	I	fit	1	iters	8	: 9.71e-01	0.045	-0.187	2.009	2.035	X = 0.0064

	az_fwhm	el_fwhm
10m antennas:	1.20 +/- 0.03	1.20 +/- 0.02
6m antennas:	1.95 +/- 0.07	1.99 +/- 0.07

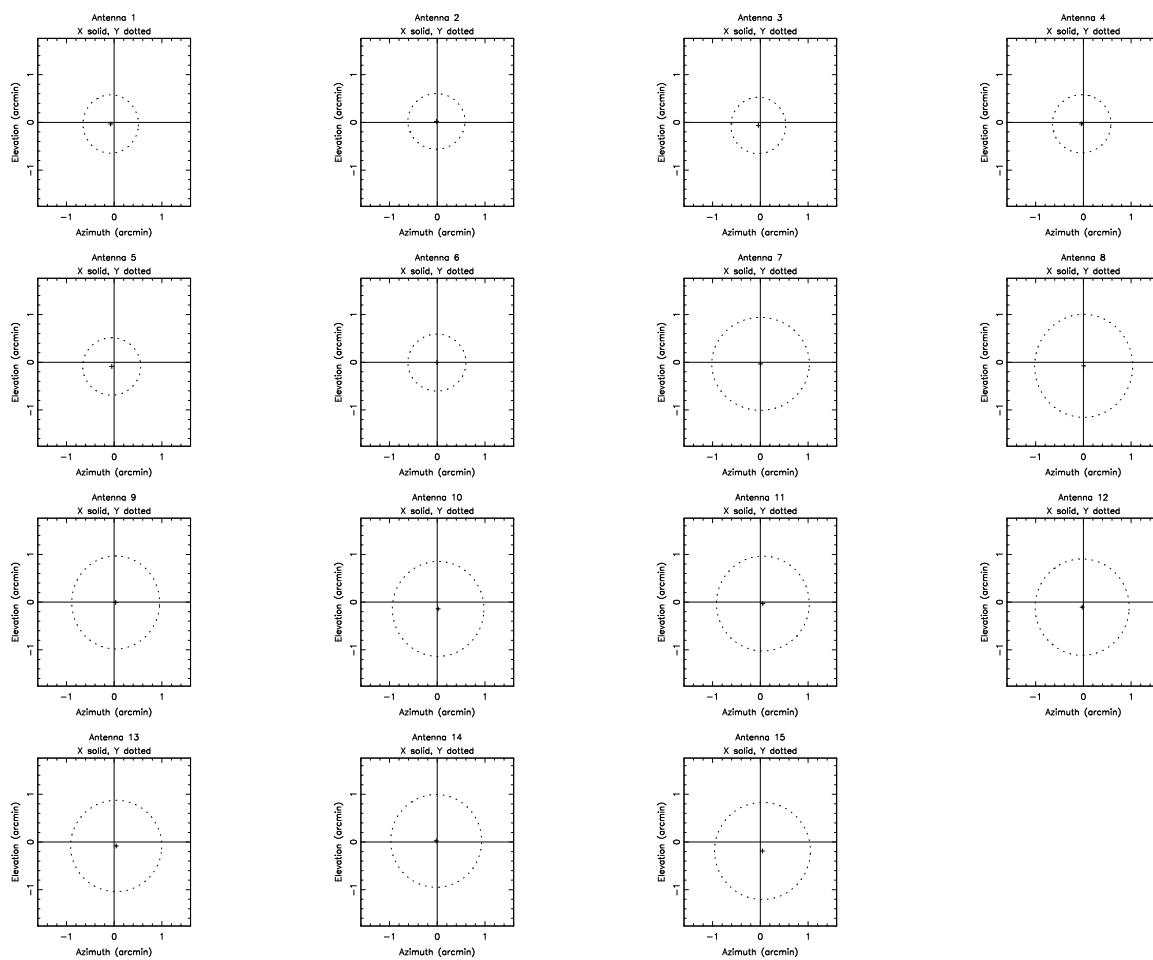


Fig. 4.— Pointing and Primary Beam FWHM at 100 GHz. File ct007.1C_1003C273.1.gpfit.0.2.ps

 Table 2. ct007.1C_1003C273.2.gpfit.0.2

#ant	pol	fit	iters	:	pkval	az_off	el_off	az_fwhm	el_fwhm	residual	
#####											
01	I	fit	1	iters	7	: 9.97e-01	0.001	-0.002	1.182	1.213	X = 0.0025
02	I	fit	1	iters	7	: 1.01e+00	-0.015	0.013	1.177	1.155	X = 0.0177
03	I	fit	1	iters	7	: 1.04e+00	-0.028	-0.015	1.183	1.163	X = 0.0033
04	I	fit	1	iters	7	: 9.83e-01	-0.039	-0.042	1.211	1.161	X = 0.0051
05	I	fit	1	iters	7	: 9.66e-01	-0.034	-0.004	1.227	1.188	X = 0.0125
06	I	fit	1	iters	7	: 9.88e-01	-0.005	0.024	1.199	1.185	X = 0.0147
07	I	fit	1	iters	8	: 9.89e-01	0.033	-0.073	1.984	1.997	X = 0.0013
08	I	fit	1	iters	8	: 9.67e-01	0.002	-0.061	2.033	1.989	X = 0.0030
09	I	fit	1	iters	8	: 9.50e-01	0.018	-0.105	1.974	1.962	X = 0.0022
10	I	fit	1	iters	8	: 9.65e-01	0.042	-0.067	1.975	1.952	X = 0.0025
11	I	fit	1	iters	8	: 9.97e-01	0.018	-0.100	1.992	1.965	X = 0.0012
12	I	fit	1	iters	8	: 9.51e-01	-0.006	-0.090	1.971	2.038	X = 0.0034
13	I	fit	1	iters	8	: 9.70e-01	0.059	-0.044	2.014	2.018	X = 0.0045
14	I	fit	1	iters	8	: 9.59e-01	0.006	-0.015	2.071	1.984	X = 0.0014
15	I	fit	1	iters	8	: 9.85e-01	0.020	-0.074	2.008	1.993	X = 0.0021

	az_fwhm	el_fwhm
10m antennas:	1.20 +/- 0.02	1.18 +/- 0.02
6m antennas:	2.00 +/- 0.03	1.99 +/- 0.03

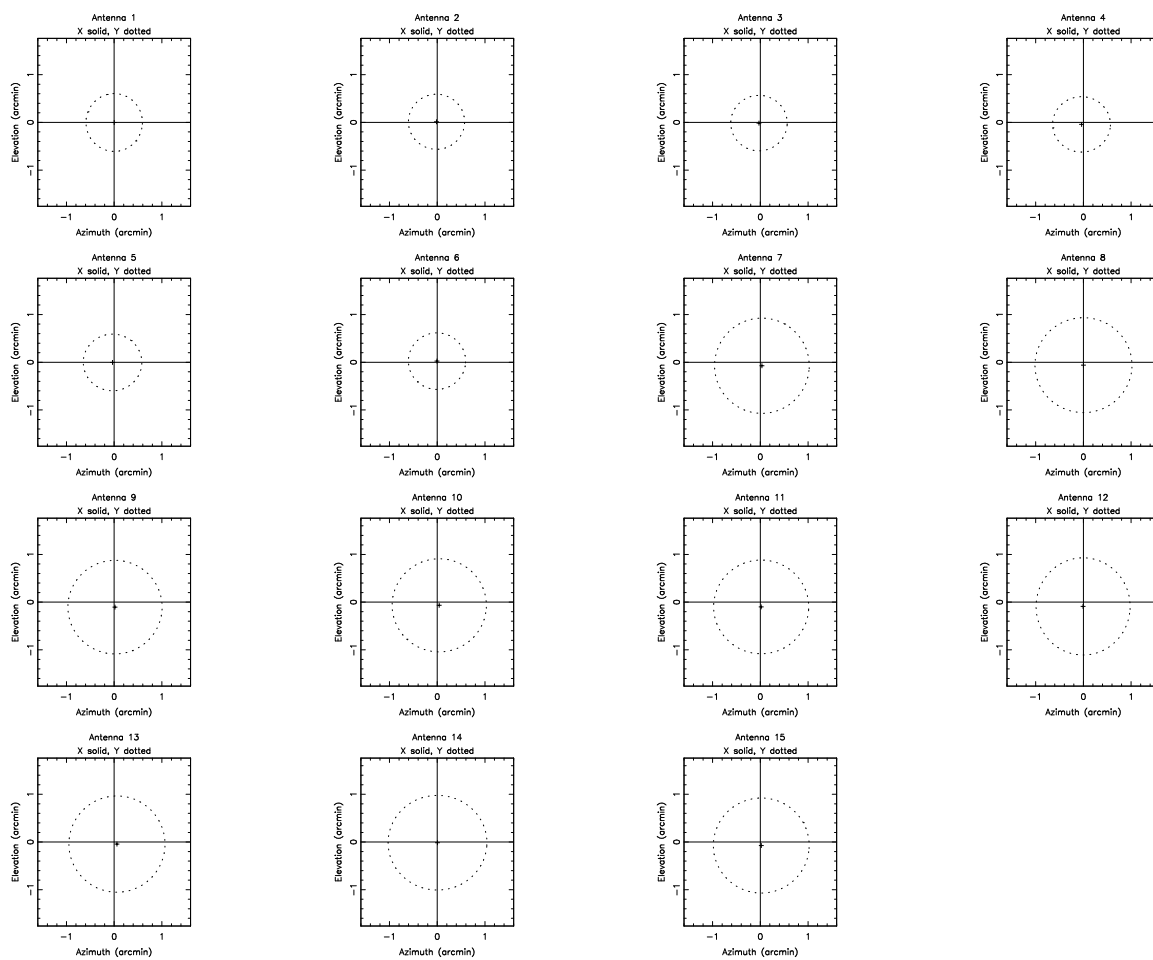


Fig. 5.— Pointing and Primary Beam FWHM at 100 GHz. File ct007.1C_1003C273.2.gpfit.0.2.ps

 Table 3. ct007.1C_2303C273.1.gpfit.60

#ant	pol	fit	iters	:	pkval	az_off	el_off	az_fwhm	el_fwhm	residual	
#####											
01	I	fit	1	iters	7	: 1.01e+00	0.008	0.009	0.545	0.521	X = 0.0369
02	I	fit	1	iters	7	: 1.05e+00	-0.009	-0.001	0.544	0.507	X = 0.0168
03	I	fit	1	iters	7	: 1.01e+00	-0.013	0.023	0.519	0.519	X = 0.0095
04	I	fit	1	iters	7	: 9.05e-01	0.025	0.020	0.554	0.524	X = 0.0112
05	I	fit	1	iters	7	: 1.01e+00	0.016	0.019	0.541	0.508	X = 0.0062
06	I	fit	1	iters	7	: 7.96e-01	0.035	-0.032	0.576	0.530	X = 0.0162
07	I	fit	1	iters	50	: 7.71e-01	10.840	-9.220	9.981	11.584	X = 0.0080
08	I	fit	1	iters	8	: 9.03e-01	-0.004	0.083	0.887	0.918	X = 0.0059
09	I	fit	1	iters	8	: 9.47e-01	-0.045	0.021	0.837	0.855	X = 0.0052
10	I	fit	1	iters	8	: 9.11e-01	-0.036	-0.013	0.843	0.868	X = 0.0011
11	I	fit	1	iters	8	: 1.01e+00	-0.007	-0.002	0.834	0.894	X = 0.0018
12	I	fit	1	iters	8	: 9.61e-01	-0.006	-0.030	0.846	0.834	X = 0.0126
13	I	fit	1	iters	8	: 9.94e-01	-0.025	-0.052	0.849	0.805	X = 0.0048
14	I	fit	1	iters	8	: 9.93e-01	0.013	0.023	0.930	0.890	X = 0.0047
15	I	fit	1	iters	8	: 8.92e-01	-0.021	0.035	0.852	0.851	X = 0.0068

Notes:

- . The Gaussian fits for ant 7 failed (iters=50)
- . Ant 6, 10, and 15 have lower aperture efficiency (lower pkval)

	az_fwhm	el_fwhm
10m antennas:	0.55 +/- 0.02	0.52 +/- 0.02
6m antennas:	0.86 +/- 0.03	0.86 +/- 0.04

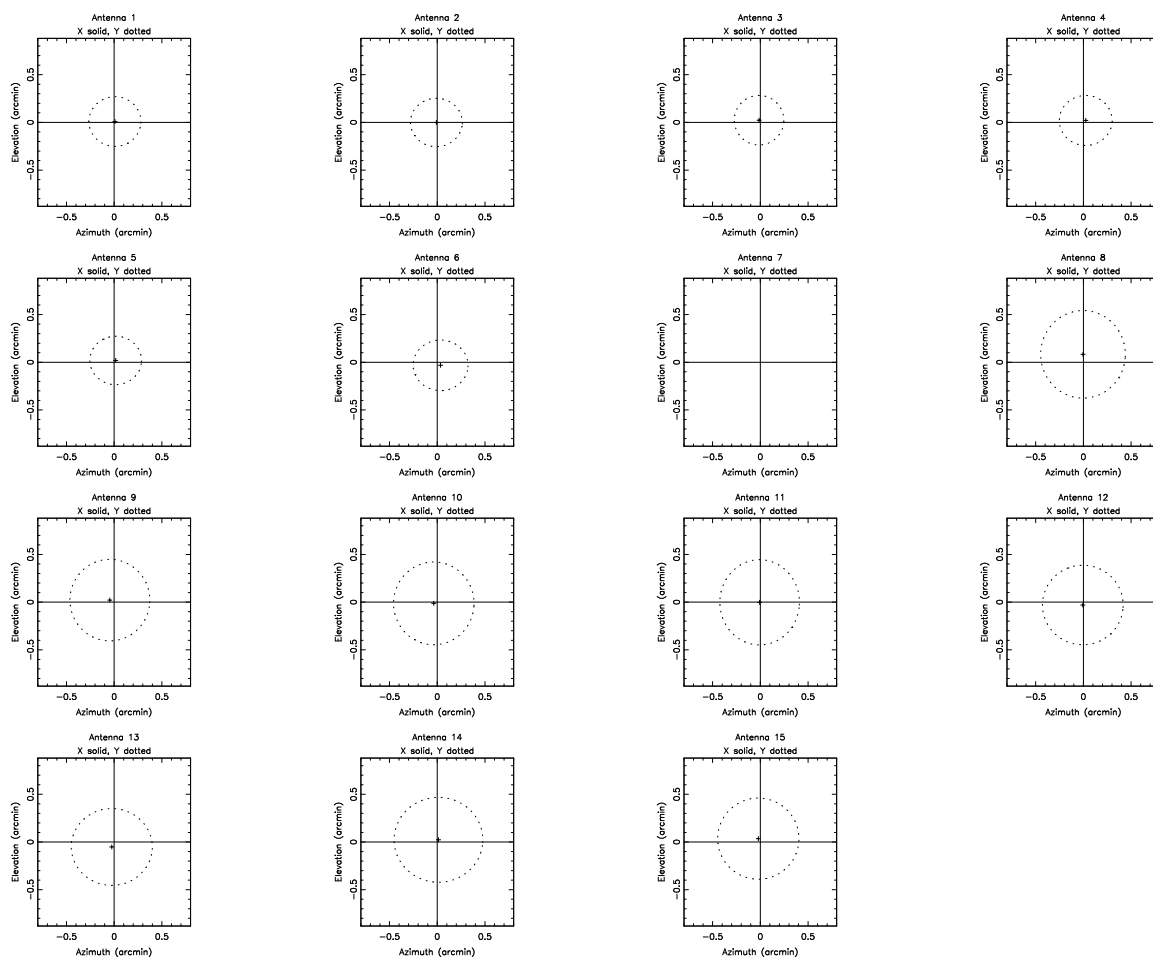


Fig. 6.— Pointing and Primary Beam FWHM at 230 GHz. File ct007.1C_2303C273.1.gpfit.60.ps

 Table 4. ct007.1C_2303C273.2.gpfit.60

#ant	pol	fit	iters	:	pkval	az_off	el_off	az_fwhm	el_fwhm	residual	
#####											
01	I	fit	1	iters	8	: 1.07e+00	-0.013	-0.037	0.510	0.485	X = 0.0391
02	I	fit	1	iters	50	: 8.36e-02	-4.176	-9.600	5.218	8.550	X = 0.0013
03	I	fit	1	iters	7	: 1.06e+00	0.062	-0.029	0.522	0.479	X = 0.0344
04	I	fit	1	iters	7	: 9.50e-01	0.055	-0.050	0.554	0.468	X = 0.0204
05	I	fit	1	iters	7	: 1.01e+00	0.055	-0.034	0.548	0.485	X = 0.0107
06	I	fit	1	iters	7	: 8.69e-01	0.028	-0.050	0.553	0.483	X = 0.0065
07	I	fit	1	iters	50	: 4.98e-01	-2.862	10.928	13.647	8.472	X = 0.0033
08	I	fit	1	iters	8	: 9.43e-01	-0.077	0.006	0.869	0.818	X = 0.0050
09	I	fit	1	iters	8	: 9.73e-01	-0.098	-0.061	0.877	0.792	X = 0.0023
10	I	fit	1	iters	8	: 9.37e-01	-0.026	-0.097	0.845	0.777	X = 0.0043
11	I	fit	1	iters	8	: 1.05e+00	-0.085	-0.015	0.844	0.823	X = 0.0048
12	I	fit	1	iters	8	: 9.89e-01	-0.034	-0.068	0.850	0.836	X = 0.0038
13	I	fit	1	iters	8	: 1.02e+00	-0.005	-0.106	0.862	0.804	X = 0.0054
14	I	fit	1	iters	8	: 1.03e+00	-0.048	-0.053	0.864	0.841	X = 0.0067
15	I	fit	1	iters	8	: 9.33e-01	-0.068	-0.022	0.879	0.818	X = 0.0070

Notes:

- . The Gaussian fits for ant 2 and 7 failed (iters=50)
- . Ant 6, 10, and 15 have lower aperture efficiency (lower pkval)

	az_fwhm	el_fwhm
10m antennas:	0.54 +/- 0.02	0.48 +/- 0.02
6m antennas:	0.86 +/- 0.01	0.81 +/- 0.02

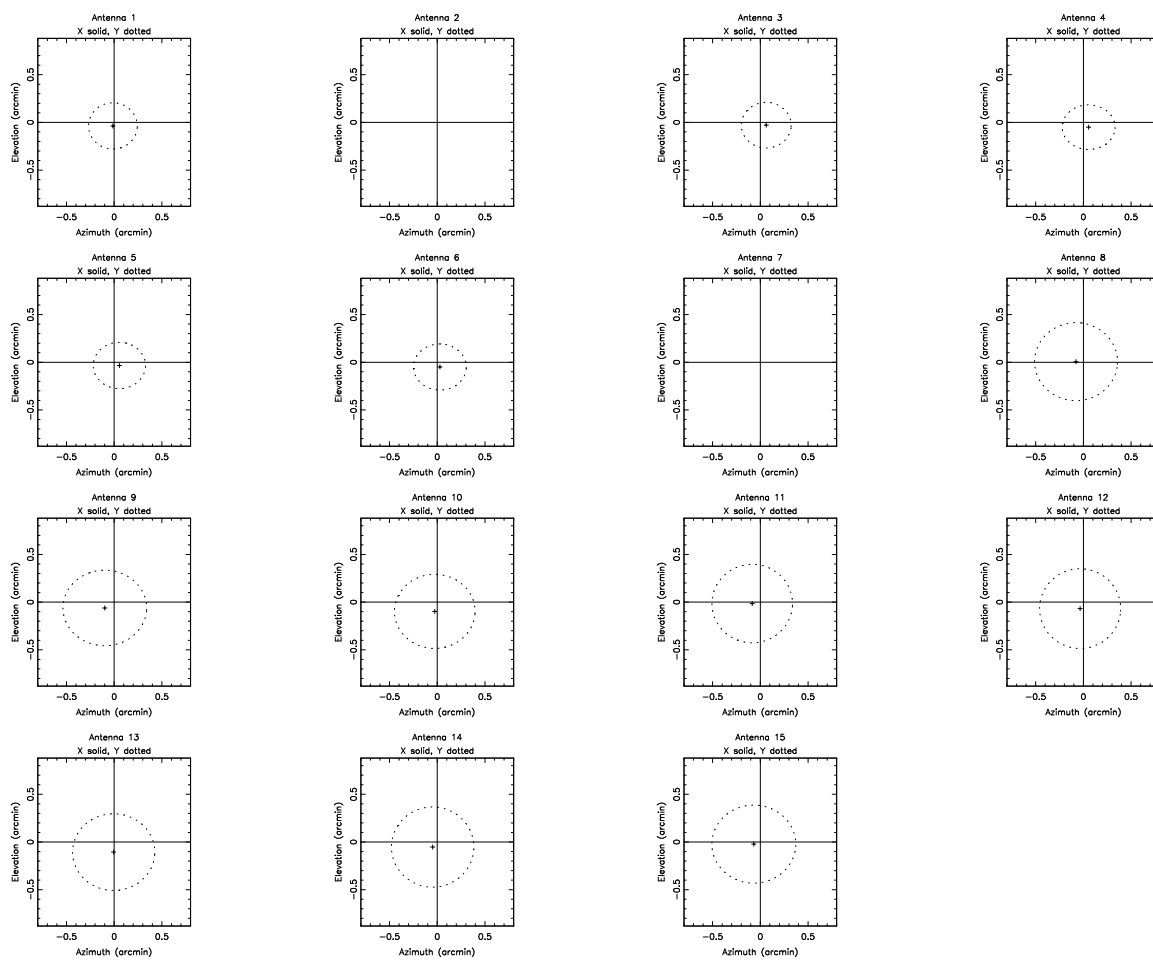


Fig. 7.— Pointing and Primary Beam FWHM at 230 GHz. File ct007.1C_2303C273.2.gpfit.60.ps

3.3. Absolute gain calibration using planet observations

In principle, we obtain an absolute gain calibration using planet observations with a planet model in selfcal. See Table 5. However, as illustrated in Figure 5, if the planet is resolved then the derived gains depend on the detailed surface brightness distribution in the planet model, and may not produce reliable fits for the aperture efficiency or primary beamwidth.

Figure 9 plots the visibility data points for the USB, and the Neptune model for the LSB at 223.0 and USB at 229.65 GHz, using a model uniform brightness disk with parameters: plangle : -23.7280, plmaj : 2.28992, plmin : 2.25076, pltb : 97.5229

For use as an absolute flux density calibration, correction, must be made for absorption lines in planetary atmospheres. We observed Neptune at 230 GHz on the CO 2-1 line. See Figure 10.

 Table 5. ct001.1C_230Neptune.2009may28

#ant	pol	fit	iters	:	pkval	az_off	el_off	az_fwhm	el_fwhm	residual
#####										
01	I	fit	1	iters	8	: 1.03e+00	-0.022	0.009	0.474	0.556 X = 0.0628
02	I	fit	1	iters	7	: 1.04e+00	0.015	-0.008	0.550	0.514 X = 0.0139
03	I	fit	1	iters	7	: 9.63e-01	-0.021	-0.010	0.503	0.498 X = 0.0254
04	I	fit	1	iters	10	: 9.56e-01	0.072	0.020	0.737	0.555 X = 0.2987
05	I	fit	1	iters	7	: 1.05e+00	0.042	-0.033	0.521	0.486 X = 0.0070
06	I	fit	1	iters	7	: 9.60e-01	0.024	-0.034	0.506	0.468 X = 0.0274
07	I	fit	1	iters	10	: 9.60e-01	-0.123	-0.043	1.283	0.790 X = 0.0448
08	I	fit	1	iters	8	: 8.79e-01	-0.150	0.167	0.764	0.761 X = 0.0084
09	I	fit	1	iters	9	: 9.53e-01	-0.022	-0.057	0.556	0.685 X = 0.0729
10	I	fit	1	iters	8	: 8.58e-01	-0.026	-0.155	0.751	0.703 X = 0.0328
11	I	fit	1	iters	9	: 9.97e-01	-0.083	-0.012	0.835	0.872 X = 0.0249
12	I	fit	1	iters	9	: 1.02e+00	0.055	-0.095	0.934	0.759 X = 0.0145
13	I	fit	1	iters	9	: 8.99e-01	0.050	-0.109	0.667	0.811 X = 0.0497
14	I	fit	1	iters	9	: 9.67e-01	-0.101	0.049	0.754	0.859 X = 0.0257
15	I	fit	1	iters	9	: 8.60e-01	-0.121	0.016	0.832	0.804 X = 0.0373

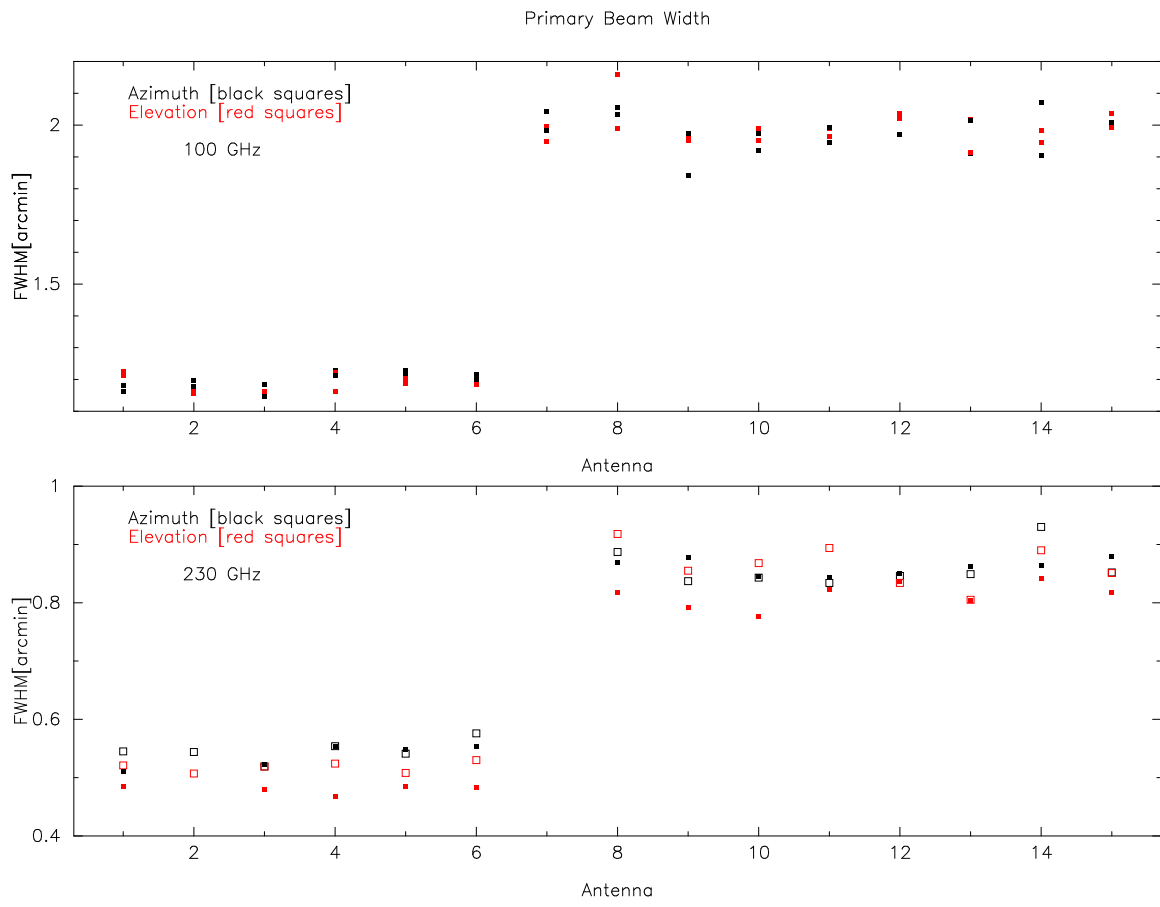


Fig. 8.— Primary Beam FWHM fitted width.

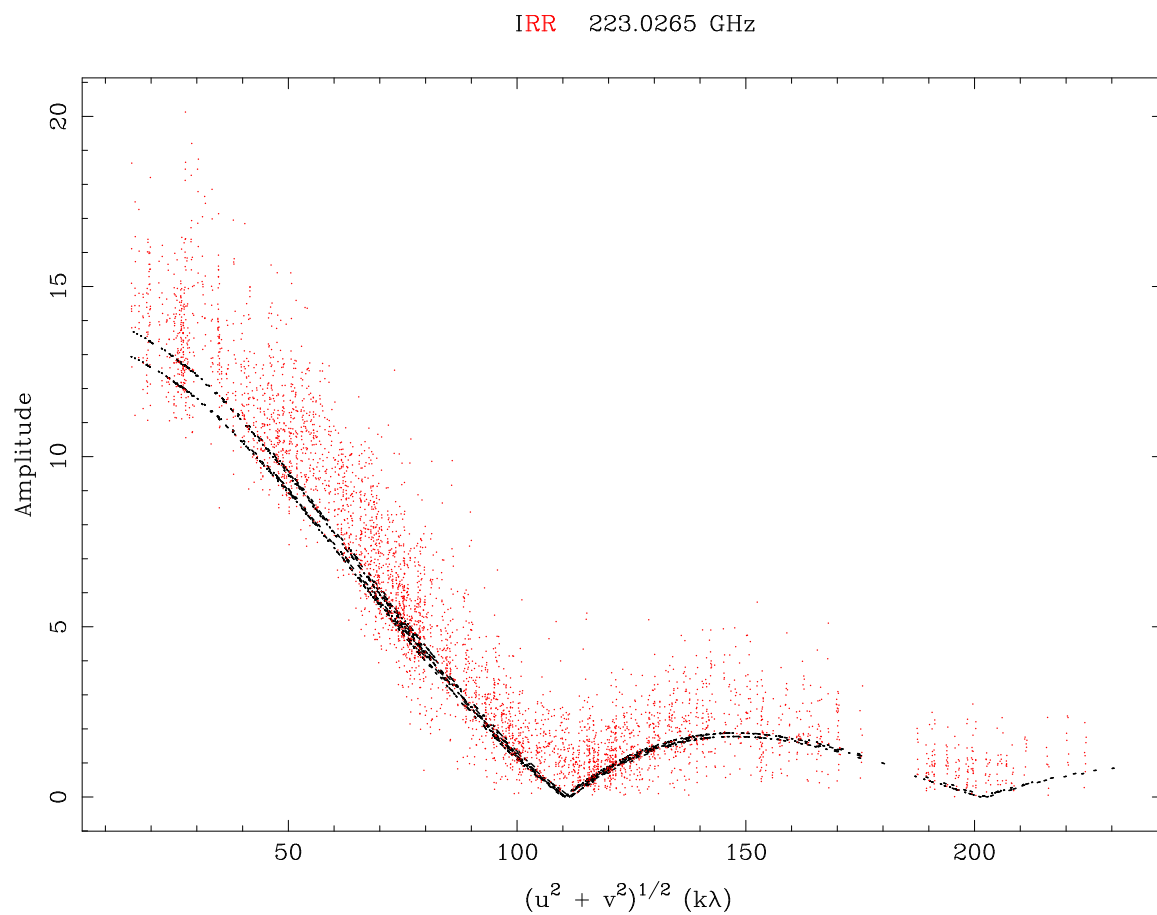


Fig. 9.— Visibility for Neptune observations at 230 GHz in the CARMA C-configuration. The solid lines show the model visibility for USB and LSB frequency.

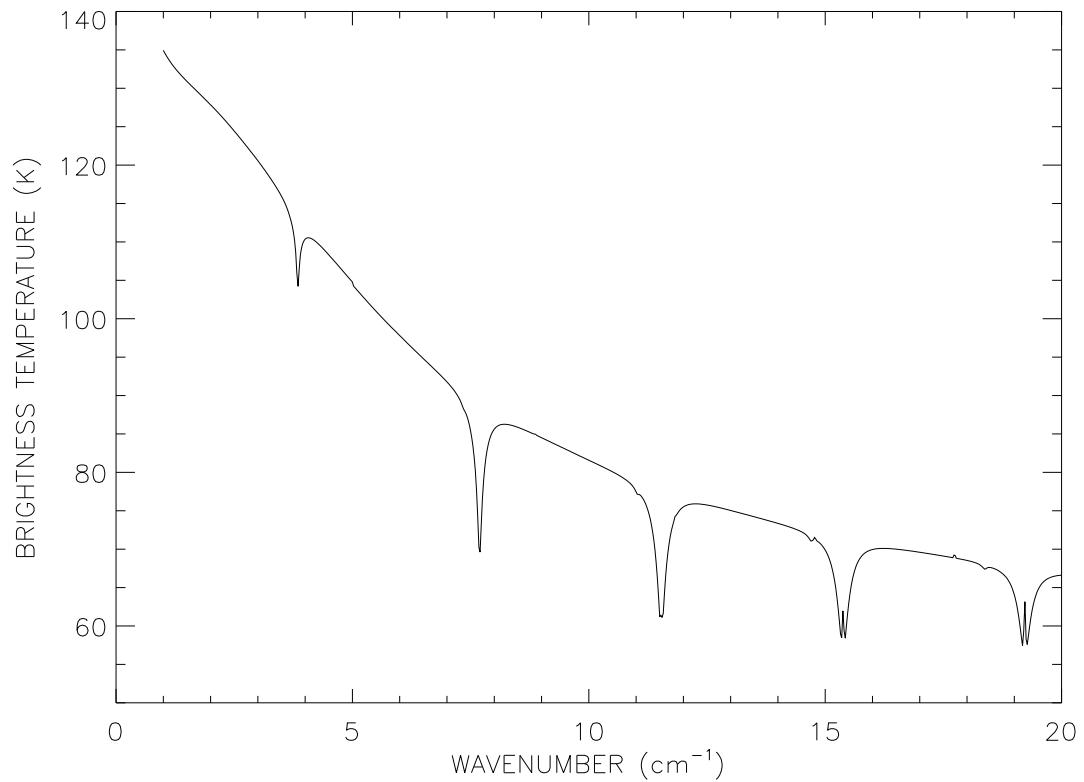


Fig. 10.— Brightness temperature of Neptune showing strong atmospheric absorption features. For use as an absolute flux density calibration, correction, must be made for absorption lines in planetary atmospheres. We often observe Neptune at 230 GHz on the CO 2-1 line!

 Table 6. 09JUN24:23:22:35.5 ct007.1E_1003C273.1.gpfit.60

#ant	pol	fit	iters	:	pkval	az_off	el_off	az_fwhm	el_fwhm	residual
#####										
01	I	fit	1	iters	8	: 9.39e-01	-0.049	0.052	1.162	1.265 X = 0.0176
02	I	fit	1	iters	8	: 9.06e-01	-0.050	0.113	1.197	1.235 X = 0.0311
03	I	fit	1	iters	7	: 9.36e-01	-0.077	0.066	1.192	1.180 X = 0.0161
04	I	fit	1	iters	8	: 9.37e-01	-0.024	0.066	1.230	1.265 X = 0.0241
05	I	fit	1	iters	8	: 8.75e-01	-0.026	0.124	1.263	1.291 X = 0.0280
06	I	fit	1	iters	8	: 9.12e-01	-0.055	0.049	1.241	1.254 X = 0.0296
07	I	fit	1	iters	8	: 8.86e-01	0.039	0.243	2.041	2.210 X = 0.0016
08	I	fit	1	iters	8	: 8.78e-01	0.079	0.063	2.007	2.086 X = 0.0048
09	I	fit	1	iters	8	: 8.83e-01	0.034	0.189	2.012	2.180 X = 0.0040
10	I	fit	1	iters	8	: 8.69e-01	-0.053	0.087	2.059	2.166 X = 0.0013
11	I	fit	1	iters	8	: 8.99e-01	0.028	0.110	1.973	2.048 X = 0.0066
12	I	fit	1	iters	8	: 8.93e-01	0.043	0.112	2.030	2.050 X = 0.0064
13	I	fit	1	iters	9	: 8.89e-01	-0.036	0.115	2.064	2.091 X = 0.0090
14	I	fit	1	iters	8	: 8.57e-01	0.048	0.124	2.070	2.128 X = 0.0051
15	I	fit	1	iters	9	: 8.90e-01	0.055	0.176	2.013	2.212 X = 0.0065

	az_fwhm	el_fwhm
10m antennas:	1.21 +/- 0.04	1.21 +/- 0.04
6m antennas:	2.03 +/- 0.03	2.13 +/- 0.06

Aperture Efficiency

Using Flux of: 3C273 09JUN02.00 at 92.3 GHz: 17.68 Jy; rms: 2.65 Jy

$$10m(100GHz) = pkval^2 \times (17.68 \pm 2.65/Flux3c273) \times 50\%$$

$$6m(100GHz) = pkval^2 \times (17.68 \pm 2.65/Flux3c273) \times 65\%$$

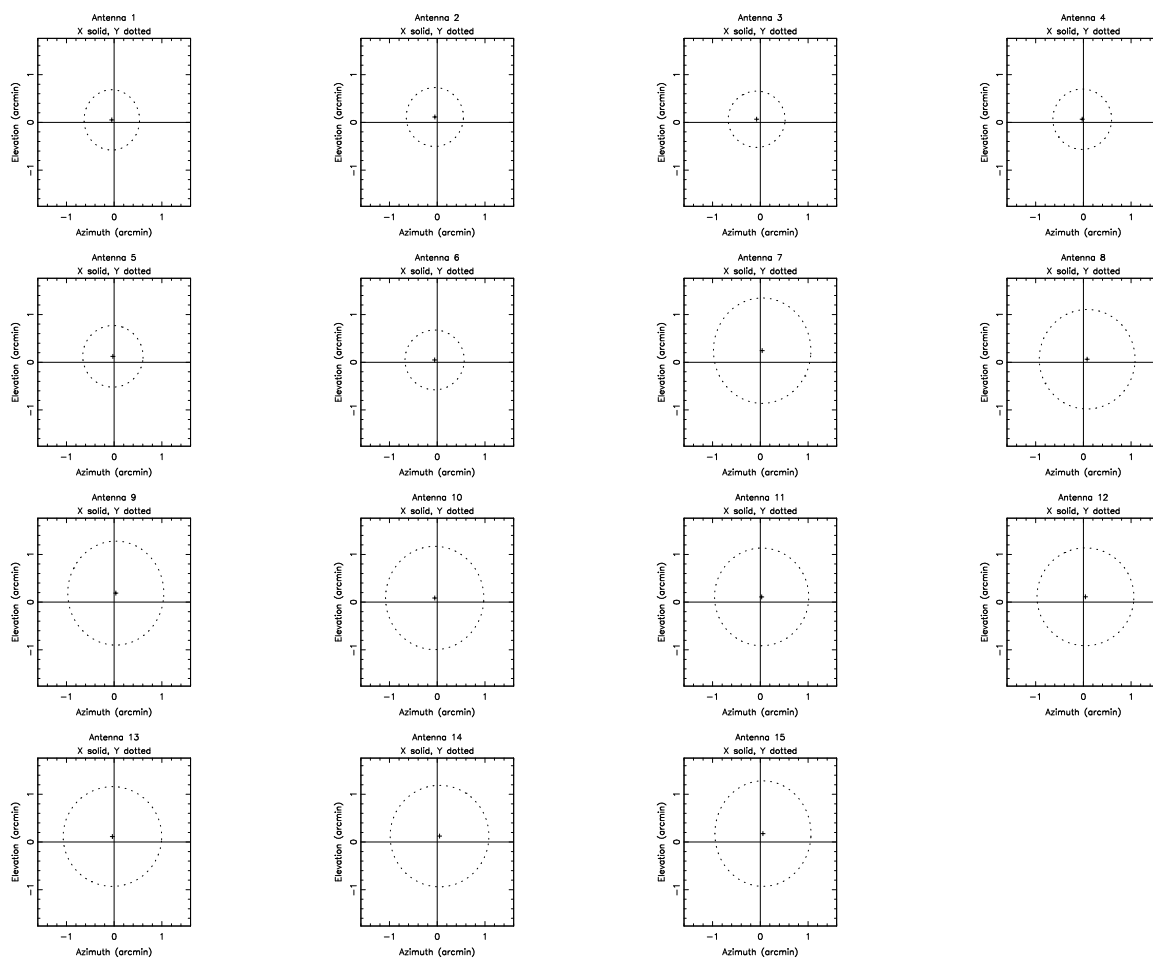


Fig. 11.— Pointing and Primary Beam FWHM at 100 GHz. File ct007.1E_1003C273.1.gpfit.60.ps

4. CONCLUSION

We used an interferometer mosaic pattern to determine the aperture efficiency, pointing, and primary beam width for the CARMA antennas at 100 and 230 GHz.

We measure antenna gains close to 65 and 145 Jy/K corresponding to aperture efficiencies 50% and 65% respectively for 10 and 6m antennas. At 230 GHz, antennas 6, 10, and 15 have lower aperture efficiency.

At 100 GHz the data are consistent with a common FWHM for azimuth and elevation axes. The average FWHM for 10m antennas is 1.20 ± 0.02 arcmin. The average for 6m antennas is 1.98 ± 0.03 arcmin. These values are significantly larger than the the current Gaussian primary beam model FWHM 1.07 and 1.92 arcmin for 10m and 6m antennas respectively. At 230 GHz the FWHM on the elevation axis appears to be smaller than on the azimuth for several of the antennas. This is possibly caused by gravitational deformation, or subreflector sag in both 6m and 10m antennas. More extensive observations at several telescope elevations are required to investigate this. The mean values are: azimuth: 0.55 ± 0.02 arcmin, elevation: 0.50 ± 0.02 arcmin for 10m antennas, and azimuth: 0.86 ± 0.02 arcmin, elevation: 0.83 ± 0.03 arcmin for 6m antennas. The current Gaussian primary beam model has the same FWHM for both axes: FWHM 0.47 and 0.83 arcmin for 10m and 6m antennas respectively.

We obtain an absolute gain calibration using planet observations with a planet model in selfcal. However, if the planet is resolved then the derived gains depend on the detailed surface brightness distribution in the planet model, and may not produce reliable fits for the aperture efficiency or primary beamwidth. For use as an absolute flux density calibration, correction, must also be made for absorption lines in planetary atmospheres.

5. References

- Cornwell, T.J., Holdaway, M.A. & Uson, J.M., 1993, A&A 271, 697, *Radio-interferometric imaging of very large objects: implications for array design*
- Holdaway, M. A., 1998, *Mosaicing with Interferometer Arrays*, in Synthesis Imaging in Radio Astronomy II, ASP Conference Series, G. B. Taylor, C. L. Carilli and R. A. Perley (eds)
- Corder, S., 2008, , PhD thesis, Caltech.
- Wright, M., 2002. CARMA memo 5, *Compact Configuration Evaluation for CARMA*
- Wright, M., 2007, CARMA memo 38 *Image Fidelity as a Function of Source Size and Calibration Errors*